Quantifying the influence of dispersion interactions on the elastic properties of crystalline cellulose

Pan Chen, Yoshiharu Nishiyama, Jakob Wohlert

Quantifying the Influence of Dispersion Interactions on the Elastic Properties of Crystalline Cellulose

Pan Chen[1*], Yoshiharu Nishiyama[2*], Jakob Wohlert[3,4*]

[1]*Beijing Engineering Research Centre of Cellulose and Its Derivatives, School of Materials Science and Engineering, Beijing Institute of Technology, 100081, Beijing, P.R. China*
[2]*Universite Grenoble Alpes, CNRS, CERMAV, 38000 Grenoble, France*
[3]*Department of Fibre and Polymer Technology, School of Engineering Sciences in Chemistry, Biotechnology and health, KTH Royal Institute of Technology, 10044 Stockholm, Sweden*
[4]*Wallenberg Wood Science Center, KTH Royal Institute of Technology, 10044 Stockholm, Sweden*
Corresponding authors: panchen@bit.edu.cn, yoshi@cermav.cnrs.fr, jacke@kth.se

Abstract

Dispersion and electrostatic interactions both contribute significantly to the tight assembly of macromolecular chains within crystalline polysaccharides. Using dispersion-corrected density functional theory (DFT) calculation, we estimated the elastic tensor of the four crystalline cellulose allomorphs whose crystal structures that are hitherto available, namely, cellulose Iα, Iβ, II, III$_I$. Comparison between calculations with and without dispersion correction allows quantification of the exact contribution of dispersion to stiffness at molecular level.

Introduction

Hydrogen bonding, London dispersion, and other electrostatic multipole interactions all play important roles in the spatial organization of molecules in crystalline polysaccharides, such as cellulose, chitin, and chitosan, which are composed of long linear ribbon-like sugar chains where hydroxyl groups are all in equatorial direction. Hydrogen bonds between hydroxyl groups are essentially electrostatic interaction between electronegative oxygen lone-pair electrons and slightly electropositive hydrogen whose electron were pulled by neighbor oxygen and can be considered as interaction between dipoles (Ramos-Cordoba et al. 2011). London dispersion interaction originates from synchronized polarization of atomic nuclei and is always attractive. Atoms in a molecule

have different electronegativity, and thus the sum of all pair-wise electrostatic interactions can be considered as multipole interactions. This is usually considered in modern molecular modeling as interaction between partial charges, which are primarily calculated using DFT method.

Understanding these interactions is of interest in the perspective of the fundamental properties of cellulose materials. One example is the process of dispersing native cellulose fiber aggregates into isolated nanofibrils or into individual polymer chains, that is, dissolution. It has often been stated that it is the “many” and “strong” inter- and intra-molecular hydrogen bonds that hinder defibrillation and dissolution of cellulose (Wang et al. 2016). A parallel can be found in the stability of double stranded DNA, which has often been explained based on the regular hydrogen bonds between opposing nucleobases in a pair. The justification to that is that a typical interaction energy of a base pair is about one order of magnitude higher than dispersion energy from an atom pair (Gooch 2007). However, recent experiments and simulations give more weight to the contribution of dispersion interaction on the stability of double helical structure, to the point that it may even exceed the hydrogen bond interaction (Černý et al. 2008; Kolář et al. 2011; Jahiruddin and Datta 2015; Perumal and Subramanian 2017; Kumar and Patwari 2019; Feng et al. 2019).

For cellulose, the industrially most important crystalline polysaccharide, the interest in how dispersion interaction influences structural stability has been revived, especially in aqueous systems where hydrophobic effects would dominate and hydrogen bonds become insignificant (Bergenstråhle et al. 2010; Medronho et al. 2012; Glasser et al. 2012). Moreover, it has been shown that the dispersion energy contribution to molecular cohesion can be twice the hydrogen bond contribution in the native cellulose crystal (Nishiyama 2018). Therefore, the influence of the different interactions on the structure and properties of cellulose needs to be re-examined.

Another example of where the relative contributions of different molecular interaction has been considered is the intrinsic mechanical properties of cellulose, which has also sometimes been attributed specifically to hydrogen bonds (Eichhorn and Davies 2006). In this case too, a parallel can be made with other biomolecules. Recently, by combining DFT calculations and nanoindentation experiments, both the types and direction of hydrogen bond were found to be correlated to the anisotropic modulus of amino acids (Azuri et al.

2015). It was concluded that the planar hydrogen bonding network co-contributed to the molecular stiffness, resulting in unusually large Young's moduli of amino acid molecular crystals along certain crystal facets. A similar trend for crystalline amino acid hydrogen maleates was reported, where the moduli can differ up to 5-fold between certain facets. (Matveychuk et al. 2018) Furthermore, by comparing DFT calculations with and without dispersion correction, the dispersion interaction was found to induce similar enhancement as hydrogen bonds to the rigidity of diphenylalanine based peptide. (Azuri et al. 2014)

The effect of hydrogen bonds on the elastic moduli of cellulose Iβ has been studied using molecular mechanics and/or molecular dynamics by switching the explicit hydrogen bond term on and off (Tashiro and Kobayashi 1985; Eichhorn and Davies 2006), in force fields that define such terms. The effect of dispersion interactions has not been studied in isolation, but the contribution from the Lennard-Jones potential, where the dispersion term is one part, was shown to be at least twice that of the contribution from electrostatics (Wohlert et al. 2012; Djahedi et al. 2015), depending on which force field that was used. The elastic tensor has been studied using first principles approach using density functional theory (Dri et al. 2013) and with thermal vibration corrections (Dri et al. 2014), but the contribution of dispersion interaction on mechanical properties has not been calculated. In quantum mechanical calculations, one cannot switch the hydrogen bonding off, but here the dispersion interaction can be simply neglected in the calculation to see its contribution. Hence, we calculated the elastic tensor of all four cellulose allomorphs using DFT to investigate the effect of dispersion interactions on their intrinsic elastic mechanical properties.

Methods

The initial atomic coordinates of crystals are imported from X-ray and neutron studies as well as molecular dynamics simulation and DFT optimization (Langan et al. 1999; Nishiyama et al. 2002, 2003; Wada et al. 2004; Chen et al. 2015). The hydrogen bonding pattern A was used for Iα and Iβ, and the pattern B was used for II and III_I. Geometry optimization was performed using the generalized gradient approximation (GGA) functional PBE (Perdew et al. 1996), augmented with pairwise DFT-D2 correction for long-range dispersion (Grimme 2006). Different k-grids are selected according to different unit cells

dimensions: 2 x 3 x 3 for I**α**, 2 x 2 x 2 for I**β** and II, and 4 x 2 x 2 for III_1. The kinetic energy cutoff was 160 Ry. The convergence threshold of total energy and forces for ionic minimization are 1.0e-6 Ry and 1.0e-5 Ry/bohr respectively. Periodic calculations were carried out using *Quantum Espresso* (version 6.6) (Giannozzi et al. 2009, 2017) in combination with *ElaStic* (Yanchitsky and Timoshevskii 2001; Golesorkhtabar et al. 2013), a universal tool for calculating elastic constants from first principles. All allomorphs except cellulose I**α** have $P2_1$ symmetry, thus the tensor was determined using the energy-stain method with 13/21 combinations of strain direction to deduce the 13/21 tensor elements (21 elements for triclinic and 13 for monoclinic). For each combination of strain, 11 points were calculated with strain amplitude up to 0.01 and the energy fitted with a parabolic function. To visualize the feature of elastic tensors, the elastic tensors were decomposed into 6 eigenvalues λ_i and 6 pairs of eigentensors of stress and strain equivalents where

$$\sigma_i = \lambda_i \varepsilon_i$$

The stress/strain tensors have 6 independent components and can be visualized in three dimension using the *PAScal* software (Cliffe and Goodwin 2012). The 3D contour surface plots were generated using the online *Anisotropic calculator* from Zuluaga *et al.* (Zuluaga 2013) and further processed using *Paraview* (Ahrens et al. 2005).

Results and discussion:

Table 1: The unit cell parameters (in Å and degrees), volume (Å^3) and *d*-spacing (Å) of crystalline cellulose from experiment (exp) and DFT calculations with dispersion correction (Disp.) or without dispersion correction (No disp.) applied. The difference in percentage is calculated either through (disp. - exp)/exp x 100% or (no disp. - exp)/exp x 100%.

		a	*b*	*C*	*α*	*β*	*γ*	*Volume*	*d-spacing*		
									110	010	100
Iα	*Exp*	10.40	6.717	5.962	80.4	118.1	114.8	333.3	3.908	5.256	6.093
	Disp.	10.40	6.564	5.857	81.7	117.2	114.1	323.9	3.828	5.200	5.984
		0.0%	-2.3%	-1.8%				-2.8%	-2.0%	-1.1%	-1.8%
	No disp.	10.46	6.920	6.920	75.9	115.5	113.2	377.0	4.376	5.666	6.344
		0.6%	3.0%	5.5%				13.1%	12.0%	7.8%	4.1%
									200	110	1-10
Iβ	*Exp (300K)*	7.784	8.201	10.38			96.5	658.3	3.867	5.314	5.959
	Disp.	7.641	8.146	10.40			96.6	636.6	3.762	5.218	5.853
		-1.8%	-0.7%	-0.2%				-2.3%	-1.8%	-1.2%	-1.4%
	No disp.	8.742	8.236	10.47			94.8	750.9	4.356	5.740	6.238
		12.3%	0.4%	0.8%				14.1%	12.6 %	8.0%	4.7%
									020	110	1-10

II	*Exp*	8.001	9.030	10.31	117.1	662.9	4.019	4.424	7.203
	Disp.	7.969	8.763	10.38	117.1	644.7	3.899	4.351	7.101
		-0.4%	-3.0%	-0.6%		-2.7%	-3.0%	-1.7%	-1.4%
	No disp.	8.100	9.476	10.44	116.5	718.4	4.246	4.601	7.362
		1.2%	4.9%	1.3%		8.4%	5.6%	4.0%	2.2%
							100	010	1-10
III_I	*Exp*	4.450	7.850	10.31	105.1	347.7	4.296	7.579	3.379
	Disp.	4.250	7.892	10.39	103.8	338.4	4.126	7.663	3.317
		-4.5%	0.5%	0.8%		-2.7%	-4.0%	-1.1%	-1.8%
	No disp.	4.711	7.868	10.45	104.8	374.3	4.554	7.606	3.530
		5.9%	0.2%	1.3%		7.7%	6.0%	0.4%	4.5%

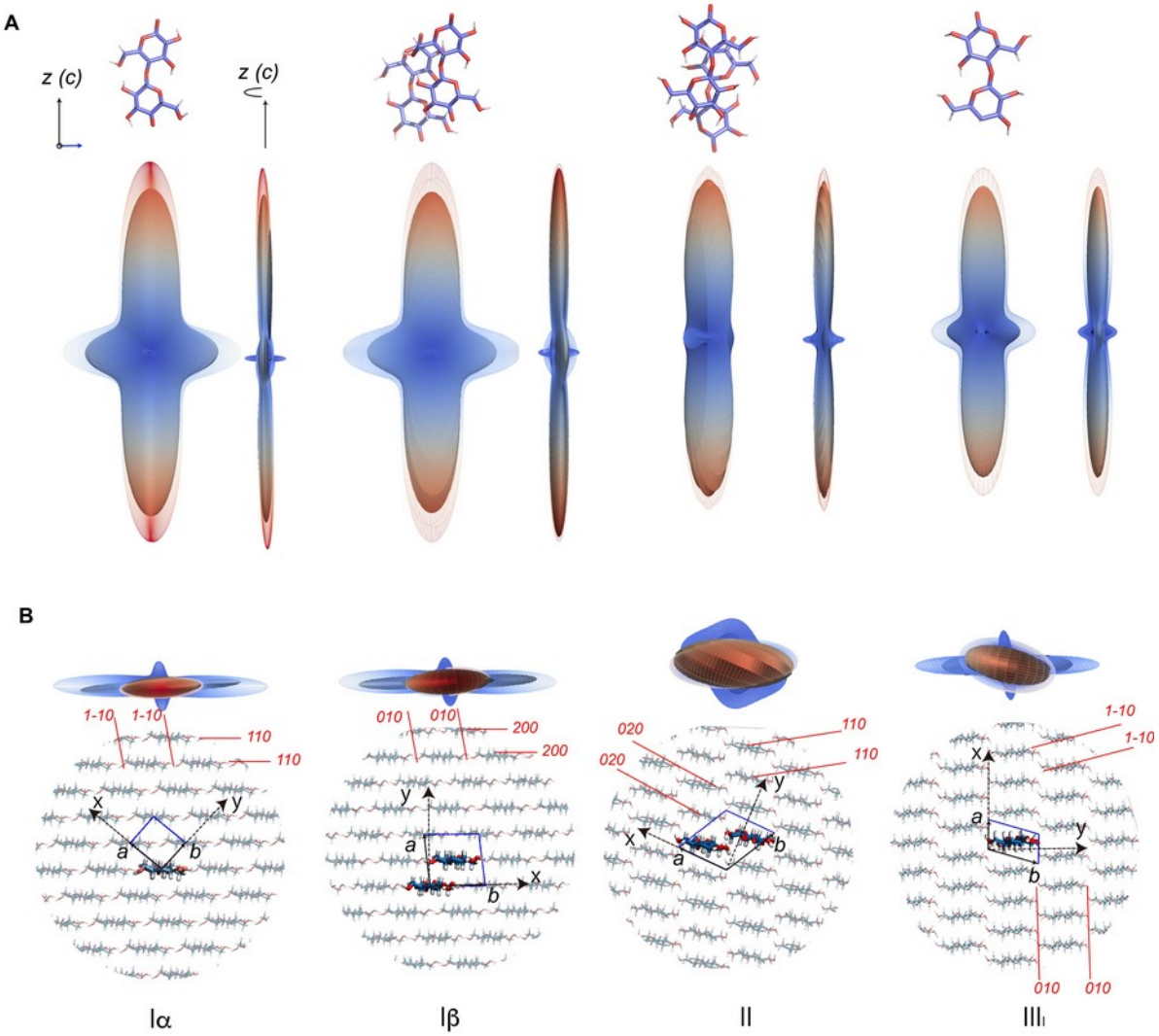

Figure 1. (A): 3D representation of the elastic moduli surface of crystalline cellulose, either with (the grid contour) or without dispersion correction (the solid contour) from two different perspectives. (B): The lateral isosurface in B is multiplied by a factor of two for I**α**, I**β**, and III_I, and by a factor of three for II for better visualization.The snapshots of the four crystalline cellulose allomorphs are labeled with unit cell and deformation vectors. The projections of cross-sections are consistent with the isosurface orientations above. Unit cell parameter *a* is parallel to x (except for I**β**, $b//\mathrm{x}$), *c* parallel to z, and y within the *ab* plane.

The influence of dispersion energy on the predicted unit cell parameters, volume, and *d*-spacing of crystalline cellulose is presented in Table 1. With the dispersion correction applied, DFT generally underestimated the experimental values by up to about 5% but can still be regarded to reproduce the experimental data within a reasonable range. This is acceptable because DFT optimized quantities represent the geometry at 0 K, whereas the experimental measurement refers to that at 300 K. Indeed, crystal structure measurements of Iβ by neutron diffraction at 15 K showed decreased unit cell dimensions compared to room temperature (Nishiyama et al. 2008), which further lowers the difference between experiment and simulation to less than 1%. In contrast, without dispersion correction, the predicted dimensions were overestimated by up to 10%. In this case, relatively large deviations can be found in the direction normal to the pyranose ring ([1 1 0] of Iα, [2 0 0] of Iβ, [0 2 0] of II, [1 1 0] and [1 -1 0] of III_I, as shown in Figure 1B). If also thermal expansion was included, the predicted values would deviate even more from experiment. Thus, dispersion interactions contribute significantly to the tight assembly of cellulose chains in the crystalline state. This is in line with a previous report where a similar strategy was used (Bučko et al. 2011).

3D contour plots of the orientation dependent Young's modulus are shown in Figure 1. The full elastic tensor in Voigt representation is given in Table 2 and the corresponding compliance tensor is presented in Table S1. Calculated values for cellulose Iβ, especially the diagonal values of stiffness tensor, is consistent with previous DFT results (Dri et al. 2013). The off-diagonal values (C_{ij}, i≠j, Table 2) are also of the same magnitude as in previous work. Cancellation of dispersion interaction resulted in a systematical reduction of the calculated values for all allomorph, varying between -4.0% to -72% for shear moduli (C44, C55, C66 in Table 1), and from -10% to -70% for tensile moduli (C11, C22, C33 in Table 1), respectively. The relative contribution of dispersion interaction on the modulus is anisotropic. It is relatively large (40% to 70 %) in the ring packing direction (010 in Iβ, 1-10 in Iα, 020 in II, and 1-10 in III_I, respectively) and small in the longitudinal chain and hydrogen bonding directions. This is expected as the covalent bonds are dominating in this direction. Still, dispersion contributes between to 5 to 17% of the Young's modulus along the chain,

which is similar to the energy decomposition analysis reported (17%) using empirical force field based molecular dynamics simulation (Wohlert et al. 2012) of cellulose Iβ.

Table 2: The stiffness tensor of crystalline cellulose from DFT calculation. (C11 of Iα and C33 of Iβ, II, and III_I are longitudinal moduli. C44, C55, and C66 are shear moduli. C22 and C33, or C11 and C22, are transverse moduli. The rest are off-diagonal elements.)

	Stiffness tensor (GPa)												
	C11	C12	C13	C14	C15	C16							
	C12	C22	C23	C24	C25	C26							
	C13	C23	C33	C34	C35	C36							
	C14	C24	C34	C44	C45	C46							
	C15	C25	C35	C45	C55	C56							
	C16	C26	C36	C46	C56	C66							
	Disp. Correction							No disp. Correction					
Iα	202.3	7.0	10.3	-1.5	0.8	1.9		167.4	2.2	2.0	-1.2	0.3	0.3
	7.0	47.8	30.7	-22.0	0.3	0.1		2.2	25.8	17.2	-18.1	0.2	-0.8
	10.3	30.7	31.0	-15.8	-1.1	0.6		2.0	17.2	14.7	-12.5	0.1	0.0
	-1.5	-22.0	-15.8	24.3	-0.4	0.0		-1.2	-18.1	-12.5	16.9	-0.1	0.2
	0.8	0.3	-1.1	-0.4	8.3	-7.4		0.3	0.2	0.1	-0.1	7.0	-6.7
	1.9	0.1	0.6	0.0	-7.4	9.4		0.3	-0.8	0.0	0.2	-6.7	9.0
Iβ	99.2	10.5	11.6	0	0	-0.4		68.2	1.5	3.4	0	0	-0.2
	10.5	17.6	9.2	0	0	-0.1		1.5	5.3	1.0	0	0	0.2
	11.6	9.2	203.6	0	0	-1.5		3.4	1.0	168.3	0	0	0.3
	0	0	0	2.1	-0.9	0		0	0	0	1.3	-0.3	0
	0	0	0	-0.9	15.7	0		0	0	0	-0.3	15.0	0
	-0.4	-0.1	-1.5	0	0	3.6		-0.2	0.2	0.3	0	0	1.0
II	37.4	17.1	3.7	0	0	0.0		41.3	13.9	5.1	0	0	-7.0
	17.1	26.5	5.3	0	0	1.8		13.9	14.4	-1.9	0	0	-2.0
	3.7	5.3	180.3	0	0	2.1		5.1	-1.9	170.9	0	0	2.4
	0	0	0	3.9	-4.0	0		0	0	0	4.8	-3.8	0
	0	0	0	-4.0	10.6	0		0	0	0	-3.8	13.1	0
	0.0	1.8	2.1	0	0	6.0		-7.0	-2.0	-2.4	0	0	8.6
III_I	22.7	20.0	8.5	0	0	-2.2		13.7	10.8	2.8	0	0	0.1
	20.0	61.0	11.9	0	0	6.2		10.8	41.4	6.9	0	0	4.9
	8.5	11.9	173.4	0	0	-1.8		2.8	6.9	152.5	0	0	-0.7
	0	0	0	11.8	-0.4	0		0	0	0	10.7	-0.1	0
	0	0	0	-0.4	3.6	0		0	0	0	-0.1	1.4	0
	-2.2	6.2	-1.8	0	0	3.6		0.1	4.9	-0.7	0	0	3.6

In the transverse directions (C22 and C33 of Iα, C11 and C22 of Iβ, II and III_I) the reduction in stiffness tensor components without dispersion correction was mostly positive,

171 which are 46% and 53% for Iα, 31% and 70% for Iβ, -10% and 46% for II, 40% and 32% for III_I,
172 respectively.

173 With dispersion correction applied, the C11 is 99.2 GPa. '1' in cellulose Iβ is the
174 direction to which both hydrogen bonding interactions and the pyranose rings are almost
175 parallel. This is much higher than the other transverse modulus, which can be ascribed to
176 the assistance of both directional hydrogen bonds and the rigidity of the glucose ring. When
177 no dispersion correction was applied, this elastic modulus drops by 30%, indicating that the
178 dispersion, in this direction, contributes to nearly one third of the total value.

179 In the sugar stacking directions, which is the directions perpendicular to the [2 0 0]
180 direction in Iβ, [1 1 0] in Iα, [0 2 0] in II, and [1 -1 0] in III_I (Figure 1), the response to
181 switching off the dispersion correction was similar, which was found to contribute 40 to
182 70% of the rigidity.

183 The dispersion correction also has significant influence on the off-diagonal elements.
184 The values of elastic tensor elements depend on the reference frame, and the standard
185 convention is to take the direction ***1*** along the *a*-axis, and direction ***2*** in the *ab*-plane (as
186 shown in Figure 2). However, the unit cell itself is not necessarily representing the principal
187 axes of physical properties. To compare the different elastic tensors in a more universal
188 way, we decomposed the elastic tensor into eigentensors that are stress/strain tensor pairs
189 that are directly related by a scalar value, the corresponding eigenvalue, which is the
190 measure of stiffness.

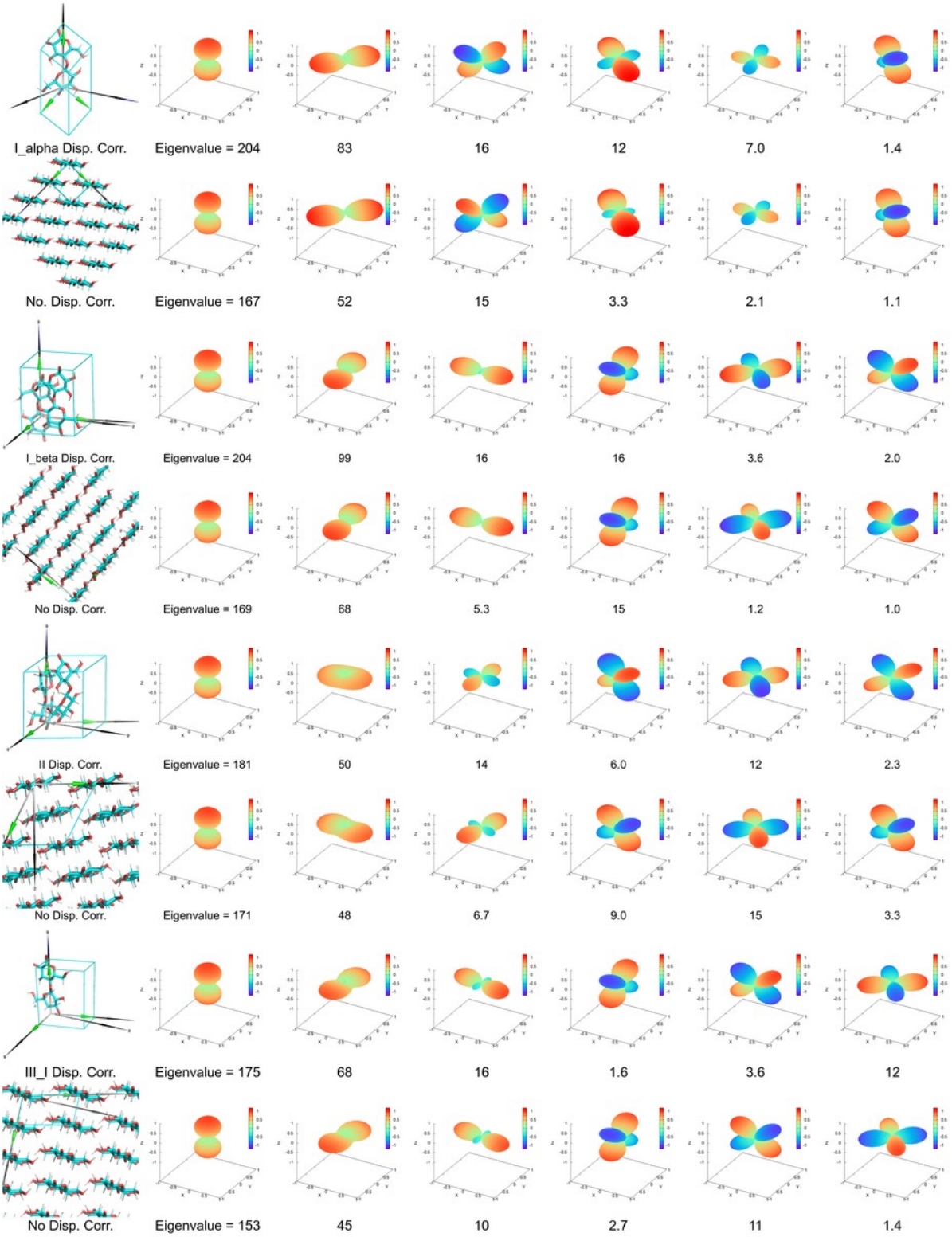

Figure 2. The 3D display of eigenvalue tensor of four cellulose allomorph with or without dispersion correction for I$\boldsymbol{\alpha}$, I$\boldsymbol{\beta}$, II, and $III_{I,}$ respectively.

196 The stress/strain tensors have 6 independent elements corresponding to axial
197 (normal) and shear stress/strain. They can be further reduced to three eigenvectors that
198 translates to a pure axial stress/strain. If the corresponding eigenvalues of all eigenvectors
199 have the same sign, they can be represented by ellipsoids, similar to thermal factor in
200 crystallographic representation. However, the stress/strain tensor can imply axial
201 stress/strain of opposite sign. Thus, we represent the tensor using color coding for positive
202 and negative values, with a surface located at a distance proportional to the axial
203 stress/strain in each direction. In general, when the mode is dominated by axial
204 stress/strain, the color is uniform, whereas shear mode shows opposite colors in orthogonal
205 directions.
206 The estimated Poisson's ratio is shown in Table S2. In comparison to experimental
207 measurements (Nakamura et al. 2004), I$\boldsymbol{\beta}$ showed slightly larger calculated $\boldsymbol{\upsilon}_{31}$ (0.49 vs. an
208 experimental value of 0.38), and II showed a smaller $\boldsymbol{\upsilon}_{32}$ (0.16 vs. 0.30).
209 To compare the elastic tensors of different allomorphs and in different conditions (with
210 and without dispersion correction), eigentensors were sorted in descending order of the
211 eigenvalue (stiffest first) of the stiffness tensor calculated with dispersion correction (first
212 row of each allomorph in Figure 2). To find the corresponding eigentensor from the
213 calculations without dispersion correction (shown on the second row), the closest
214 eigentensor was chosen, based on a distance measure. This distance was calculated as an
215 inner product, which is 1 when they match perfectly, and 0 when orthogonal. The
216 corresponding structure is drawn in the same reference frame.
217 Figure 2 shows that in all cases the highest eigenvalue is dominated by axial
218 deformation along the chain direction, which was already seen from the diagonal elements
219 of the stiffness tensor.
220 For cellulose Iβ the eigentensors following the first one have a straightforward
221 interpretation. The second eigentensor is axial deformation almost parallel to the *y*-axis.
222 This is the direction of inter-molecular hydrogen bonding, parallel to the pyranose plane.
223 The third one is orthogonal to the two, followed by three shear modes: *yz*, *xy*, and *xz*.
224 The fact that, considering lateral directions only, the structure is stiffest in the direction
225 of inter-molecular hydrogen bonding is often discussed as manifestation of the effect of
226 hydrogen bonding. However, it should be remembered that the density of covalent bonds is

higher in this direction (along unit cell *b* of Iβ in Figure 1B), while the non-covalent interactions appears only every 8 Å (d_{010} = 0.82 nm), compared to every 4 Å (d_{200} = 0.39 nm) in the perpendicular direction. Since a typical stable non-bonded separation is of the order of 3 Å, properties perpendicular to the pyranose ring plane are dominated by non-bonded interactions. In the hydrogen bonded plane ([2 0 0] of Iβ), atoms are mostly linked through covalent bonds, contributing to the high rigidity.

For cellulose II and III_I, still only considering lateral directions, the tensile deformation in the pyranose plane is highly coupled to its perpendicular direction and, in the case of cellulose II the second eigentensor almost appears as elongated doughnuts when dispersion correction is on. This tendency can be also verified in the off-diagonal element value that are similar to the diagonal element in *x* and *y* directions. The axial deformation in the direction perpendicular to the pyranose plane is coupled to *xy* shear (3rd tensor). At first sight, one would tend to interpret this feature as due to a zig-zag hydrogen bond pattern leading to a honeycomb-like response, but the fact that the dispersion correction enhances this tendency suggests that the mechanism is more complex and requires further clarification.

The eigentensors of cellulose Iα is strikingly different from Iβ, except for the stiffest mode. The deformation of a material is dominated by soft components, and thus cellulose Iα and Iβ would behave quite differently in complex stress environment in a dense material.

Conclusion:

We have systematically calculated unit cell parameters and elastic moduli of four crystalline cellulose allomorphs using DFT. The influence of the dispersion energy on both crystal structures and elastic constants was investigated by switching the dispersion correction on and off. Our calculations reveal that the dispersion interactions dominate the stacking of cellulose chains, in all crystal forms, especially in the direction perpendicular to the pyranose rings ([2 0 0] in I**β**, [1 1 0] in I**α**, [0 2 0] in II, and [1 -1 0] in III_I, respectively). In this direction, dispersion energy contributes more than 50% to the elastic mechanical properties. It further contributes about one third in the hydrogen bonding direction ([2 0 0] in I**β**, [1 1 0] in I**α**, [0 2 0, 1 1 0] in II, and [1 -1 0, 1 1 0] in III_I, respectively), and 5 to 17% in the chain direction. These findings emphasize that dispersion energy contributes

significantly to the mechanical properties of cellulose, and they also indicate that the contribution from dispersion energy exceeds that of hydrogen bonding during the initial step of defibrillation or dissolution of cellulose.

Acknowledgements:

P.C. thanks the Beijing Natural Science Foundation (2204096) and Beijing Institute of Technology Research Fund for Young Scholars. Partial computational resources were provided by the Swedish National Infrastructure for Computing (SNIC) at the PDC Center for High Performance Computing, KTH Royal Institute of Technology, partially funded by the Swedish Research Council through grant agreement no. 2018-05973.

Declaration:

The authors declare that they have no conflicts of interest. No animal or human trials were undertaken or conducted for this study. All the three authors are aware of the submission and have given their consent to participate. All the authors have read and approved the manuscript before submission.

References:

Ahrens J, Geveci B, Law C (2005) ParaView: An End-User Tool for Large Data Visualization, Visualization Handbook. Elsevier

Azuri I, Adler-Abramovich L, Gazit E, et al (2014) Why Are Diphenylalanine-Based Peptide Nanostructures so Rigid? Insights from First Principles Calculations. J Am Chem Soc 136:963–969. https://doi.org/10.1021/ja408713x

Azuri I, Meirzadeh E, Ehre D, et al (2015) Unusually Large Young's Moduli of Amino Acid Molecular Crystals. Angew Chem Int Ed 54:13566–13570. https://doi.org/10.1002/anie.201505813

Bergenstråhle M, Wohlert J, Himmel ME, Brady JW (2010) Simulation studies of the insolubility of cellulose. Carbohydr Res 345:2060–2066. https://doi.org/10.1016/j.carres.2010.06.017

Bučko T, Tunega D, Ángyán JG, Hafner J (2011) Ab Initio Study of Structure and Interconversion of Native Cellulose Phases. J Phys Chem A 115:10097–10105. https://doi.org/10.1021/jp205827y

Černý J, Kabeláč M, Hobza P (2008) Double-Helical → Ladder Structural Transition in the B-DNA is Induced by a Loss of Dispersion Energy. J Am Chem Soc 130:16055–16059. https://doi.org/10.1021/ja805428q

Chen P, Ogawa Y, Nishiyama Y, et al (2015) Alternative hydrogen bond models of cellulose II and IIII based on molecular force-fields and density functional theory. Cellulose 22:1485–1493. https://doi.org/10.1007/s10570-015-0589-z

Cliffe MJ, Goodwin AL (2012) PASCal: a principal axis strain calculator for thermal expansion and compressibility determination. J Appl Crystallogr 45:1321–1329. https://doi.org/10.1107/S0021889812043026

Djahedi C, Berglund LA, Wohlert J (2015) Molecular deformation mechanisms in cellulose allomorphs and the role of hydrogen bonds. Carbohydr Polym 130:175–182. https://doi.org/10.1016/j.carbpol.2015.04.073

Dri FL, Hector LG, Moon RJ, Zavattieri PD (2013) Anisotropy of the elastic properties of crystalline cellulose Iβ from first principles density functional theory with Van der Waals interactions. Cellulose 20:2703–2718. https://doi.org/10.1007/s10570-013-0071-8

Dri FL, Shang S, Hector LG, et al (2014) Anisotropy and temperature dependence of structural, thermodynamic, and elastic properties of crystalline cellulose I$\upbeta$: a first-principles investigation. Model Simul Mater Sci Eng 22:085012. https://doi.org/10.1088/0965-0393/22/8/085012

Eichhorn SJ, Davies GR (2006) Modelling the crystalline deformation of native and regenerated cellulose. Cellulose 13:291–307. https://doi.org/10.1007/s10570-006-9046-3

Feng B, Sosa RP, Mårtensson AKF, et al (2019) Hydrophobic catalysis and a potential biological role of DNA unstacking induced by environment effects. Proc Natl Acad Sci 116:17169–17174. https://doi.org/10.1073/pnas.1909122116

Giannozzi P, Andreussi O, Brumme T, et al (2017) Advanced capabilities for materials modelling with Quantum ESPRESSO. J Phys Condens Matter 29:465901. https://doi.org/10.1088/1361-648X/aa8f79

Giannozzi P, Baroni S, Bonini N, et al (2009) QUANTUM ESPRESSO: a modular and open-source software project for quantum simulations of materials. J Phys Condens Matter 21:395502. https://doi.org/10.1088/0953-8984/21/39/395502

Glasser WG, Atalla RH, Blackwell J, et al (2012) About the structure of cellulose: debating the Lindman hypothesis. Cellulose 19:589–598. https://doi.org/10.1007/s10570-012-9691-7

Golesorkhtabar R, Pavone P, Spitaler J, et al (2013) ElaStic: A tool for calculating second-order elastic constants from first principles. Comput Phys Commun 184:1861–1873. https://doi.org/10.1016/j.cpc.2013.03.010

Gooch JW (ed) (2007) London dispersion forces (London forces). In: Encyclopedic Dictionary of Polymers. Springer, New York, NY, pp 582–582

Grimme S (2006) Semiempirical GGA-type density functional constructed with a long-range dispersion correction. J Comput Chem 27:1787–1799. https://doi.org/10.1002/jcc.20495

Jahiruddin S, Datta A (2015) What Sustains the Unnatural Base Pairs (UBPs) with No Hydrogen Bonds. J Phys Chem B 119:5839–5845. https://doi.org/10.1021/acs.jpcb.5b03293

Kolář M, Kubař T, Hobza P (2011) On the Role of London Dispersion Forces in Biomolecular Structure Determination. J Phys Chem B 115:8038–8046. https://doi.org/10.1021/jp202878d

Kumar A, Patwari GN (2019) Probing the role of dispersion energy on structural transformation of double-stranded xylo- and ribo-nucleic acids. Phys Chem Chem Phys 21:3842–3848. https://doi.org/10.1039/C8CP06305B

Langan P, Nishiyama Y, Chanzy H (1999) A Revised Structure and Hydrogen-Bonding System in Cellulose II from a Neutron Fiber Diffraction Analysis. J Am Chem Soc 121:9940–9946. https://doi.org/10.1021/ja9916254

Matveychuk YV, Bartashevich EV, Tsirelson VG (2018) How the H-Bond Layout Determines Mechanical Properties of Crystalline Amino Acid Hydrogen Maleates. Cryst Growth Des 18:3366–3375. https://doi.org/10.1021/acs.cgd.8b00067

Medronho B, Romano A, Miguel MG, et al (2012) Rationalizing cellulose (in)solubility: reviewing basic physicochemical aspects and role of hydrophobic interactions. Cellulose 19:581–587. https://doi.org/10.1007/s10570-011-9644-6

Nakamura K, Wada M, Kuga S, Okano T (2004) Poisson's ratio of cellulose Iβ and cellulose II. J Polym Sci Part B Polym Phys 42:1206–1211

Nishiyama Y (2018) Molecular interactions in nanocellulose assembly. Philos Trans R Soc Math Phys Eng Sci 376:20170047. https://doi.org/10.1098/rsta.2017.0047

Nishiyama Y, Johnson GP, French AD, et al (2008) Neutron Crystallography, Molecular Dynamics, and Quantum Mechanics Studies of the Nature of Hydrogen Bonding in Cellulose Iβ. Biomacromolecules 9:3133–3140. https://doi.org/10.1021/bm800726v

Nishiyama Y, Langan P, Chanzy H (2002) Crystal Structure and Hydrogen-Bonding System in Cellulose Iβ from Synchrotron X-ray and Neutron Fiber Diffraction. J Am Chem Soc 124:9074–9082. https://doi.org/10.1021/ja0257319

Nishiyama Y, Sugiyama J, Chanzy H, Langan P (2003) Crystal Structure and Hydrogen Bonding System in Cellulose Iα from Synchrotron X-ray and Neutron Fiber Diffraction. J Am Chem Soc 125:14300–14306. https://doi.org/10.1021/ja037055w

Perdew JP, Burke K, Ernzerhof M (1996) Generalized Gradient Approximation Made Simple. Phys Rev Lett 77:3865–3868. https://doi.org/10.1103/PhysRevLett.77.3865

Perumal SSRR, Subramanian Y (2017) A molecular dynamics calculation of solid phase of malonic acid: role of hydrogen-bond chains and the elastic constants. J Chem Sci 129:963–974. https://doi.org/10.1007/s12039-017-1310-6

Ramos-Cordoba E, Lambrecht DS, Head-Gordon M (2011) Charge-transfer and the hydrogen bond: Spectroscopic and structural implications from electronic structure calculations. Faraday Discuss 150:345–362. https://doi.org/10.1039/C1FD00004G

Tashiro K, Kobayashi M (1985) Calculation of crystallite modulus of native cellulose. Polym Bull 14:213–218. https://doi.org/10.1007/BF00254940

Wada M, Chanzy H, Nishiyama Y, Langan P (2004) Cellulose IIII Crystal Structure and Hydrogen Bonding by Synchrotron X-ray and Neutron Fiber Diffraction. Macromolecules 37:8548–8555. https://doi.org/10.1021/ma0485585

Wang S, Lu A, Zhang L (2016) Recent advances in regenerated cellulose materials. Prog Polym Sci 53:169–206. https://doi.org/10.1016/j.progpolymsci.2015.07.003

Wohlert J, Bergenstråhle-Wohlert M, Berglund LA (2012) Deformation of cellulose nanocrystals: entropy, internal energy and temperature dependence. Cellulose 19:1821–1836. https://doi.org/10.1007/s10570-012-9774-5

Yanchitsky BZ, Timoshevskii AN (2001) Determination of the space group and unit cell for a periodic solid☆☆This program can be downloaded from the CPC Program Library under catalogue identifier: http://cpc.cs.qub.ac.uk/summaries/ADON. Comput Phys Commun 139:235–242. https://doi.org/10.1016/S0010-4655(01)00212-0

Zuluaga M (2013) Anisotropy Calculator - 3D Visualization Toolkit. https://doi.org/10.4231/D3JD4PQ2D